

Document downloaded from:

<http://hdl.handle.net/10251/148913>

This paper must be cited as:

Rutkowska, M.; Pacia, I.; Basag, S.; Kowalczyk, A.; Piwowarska, Z.; Duda, M.; Tarach, K.... (2017). Catalytic performance of commercial Cu-ZSM-5 zeolite modified by desilication in NH₃-SCR and NH₃-SCO processes. *Microporous and Mesoporous Materials*. 246:193-206. <https://doi.org/10.1016/j.micromeso.2017.03.017>



The final publication is available at

<https://doi.org/10.1016/j.micromeso.2017.03.017>

Copyright Elsevier

Additional Information

Catalytic performance of commercial Cu-ZSM-5 zeolite modified by desilication in NH₃-SCR and NH₃-SCO processes

M. Rutkowska, I. Pacia, S. Basag, A. Kowalczyk, Z. Piwowarska, M. Duda, K.A. Tarach, K. Gora-Marek, M. Michalik, U. Díaz, L. Chmielarz

Abstract

In the presented manuscript an influence of the mesoporosity generation in commercial ZSM-5 zeolite on its catalytic performance in two environmental processes, such as NO reduction with ammonia (NH₃-SCR, Selective Catalytic Reduction of NO with NH₃) and NH₃ oxidation (NH₃-SCO, Selective Catalytic Oxidation of NH₃) was examined. Micro-mesoporous catalysts with the properties of ZSM-5 zeolite were obtained by desilication with NaOH and NaOH/TPAOH (tetrapropylammonium hydroxide) mixture with different ratios (TPA⁺/OH⁻ = 0.2, 0.4, 0.6, 0.8 and ∞) and for different durations (1, 2, 4 and 6 h). The results of the catalytic studies (over the Cu-exchanged samples) showed higher activity of this novel mesostructured group of zeolitic materials. Enhanced catalytic performance was related to the generated mesoporosity (improved Hierarchy Factor (HF) of the samples), that was observed especially with the use of Pore Directing Agent (PDA) additive, TPAOH. Applied desilication conditions did not influence significantly the crystallinity of the samples (X-ray diffraction analysis (XRD)), despite the treatment for 6 h in NaOH solution, which was found to be too severe to preserve the zeolitic properties of the samples. The modified porous structure and accessibility of acid sites (increased surface acidity determined by temperature programmed desorption of ammonia (NH₃-TPD)) influenced the red-ox properties of copper species introduced by ion-exchange method (temperature programmed reduction with hydrogen (H₂-TPR). Increased acidity of the micro-mesoporous samples, as well as the content of easily reducible copper species resulted in a significant improvement of Cu-ZSM-5 catalytic efficiency in the NH₃-SCR and NH₃-SCO processes.

Graphical abstract

Image 1

[Download high-res image \(192KB\)](#)[Download full-size image](#)

[Previous article in issue](#)

[Next article in issue](#)

Keywords

ZSM-5

Desilication

Pore directing agent

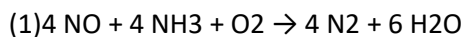
NH3-SCR

NH3-SCO

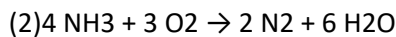
1. Introduction

Nitrogen oxides, NO_x (NO and NO₂), emitted during combustion of fossil fuels are considered as one of the most dangerous air pollutants. Majority of NO_x emission comes from transportation sector, from both gasoline and diesel engines. The current European standard regulations for NO_x emission (Euro 6; 2014-2020) established the limits as 0.06 g/km (gasoline engine) and 0.08 g/km (diesel engine) [1]. Continuously growing air pollution and a need to fulfill the new law regulations are a reason of high scientist interest in the research on catalyst for three-way and lean-burn DeNO_x processes.

Diesel engines are a source of higher NO_x emission in comparison to gasoline ones and selective catalytic reduction (DeNO_x) of nitrogen oxides with NH₃ is considered as one of the most promising technologies for NO_x abatement [2,3]. The typical NO/NO₂ ratio in diesel exhaust gases is about 9, thus the main NH₃-SCR reaction can be presented as Eq. (1)[2].



The application of the NH₃-SCR technology in diesel engines involves a danger of unreacted ammonia slip resulting from urea overdosing. Thus, to avoid the emission of toxic ammonia the second catalyst bed for NH₃ selective catalytic oxidation should be applied in the catalytic converter [4] (Eq. (2)).



One of the possible solutions for the elimination of NO_x emission and ammonia slip from the diesel automotive waste gases is the application of catalyst active in both the processes, which are recognized as proceeding in different temperature ranges [5].

Zeolites modified with Cu (e.g. with MFI, BEA or CHA topology [6–8]) due to their high catalytic activity at low operating temperatures (typical of diesel exhaust gases), are under high interest for the application in diesel emission control [9]. The novel trends in the development of the zeolitic materials aim to overcome the diffusion limitations (caused by the presence of micropores) and to enhance the accessibility of the catalytically active centers [10–12]. One of the possible modifications of the zeolite structure, leading to an increase in catalytic efficiency, is the generation of mesopores.

The investigations on the catalytic efficiency of mesoporous zeolites in the DeNO_x process showed their higher activity and stability in comparison to conventional microporous zeolites. Zeolites with the hierarchical porous structure were found to be more active at high

temperatures (at which conventional zeolites promote ammonia oxidation) and in long term stability tests [13–18]. Various mesoporous zeolites with different pore structure, such as ZSM-5 [13–17], ZSM-12 [17], ITQ-2 or MCM-36 [18] were examined in the NH₃-SCR process.

Mesoporosity in zeolites can be generated by different methods, however, among them desilication seems to be one of the cheapest and easiest. Thus, the application of this approach in a large-scale catalyst production is very promising. Desilication (base leaching) is a post-synthesis method basing on the zeolite treatment in alkaline medium (e.g. solution of NaOH or Na₂CO₃). Ma et al. [15] and Vennestrøm et al. [16] investigated the catalytic activity of iron modified ZSM-5 desilicated with sodium and guanidinium hydroxides, respectively. In both cases the mesoporosity generation resulted in an increase of NO conversion in a broad temperature range in comparison to conventional zeolite.

The main drawback of desilication is a formation of mesopores at the expense of microporosity. In order to optimize the interplay between enhanced mesopore surface area (accessibility function) and micropore volume (catalytic performance) Pérez-Ramírez et al. [19] reported a novel desilication method with the usage of pore directing agent. In this method besides NaOH simultaneously quaternary ammonium cations (such as TMA⁺, TPA⁺ or TBA⁺) are used. Pore directing agents act as pore-growth moderators and reduce the effect of zeolite crystals leaching, resulting in better preserved intrinsic zeolite properties. Verboekend et al. [20] examined various quaternary ammonium cations and amines in mesopores formation in USY and Beta zeolites and found that their influence on desilication depends on PDAs charge and size. Moreover, the results showed that depending on the concentration of PDA the external surface and mesopore size can be tuned. Sadowska et al. [21–23] investigated desilication of ZSM-5 zeolite with NaOH of different concentrations and with NaOH/TBAOH mixtures of various ratios between bases. Hierarchical zeolites obtained with the use of NaOH and TBAOH were characterized by mesopores of higher volume and surface area, but with smaller diameter than in case of the use of NaOH.

In the presented studies commercial ZSM-5 zeolite was chosen for the modification by desilication, in order to obtain more adequate results for the possible future scaling-up of the process. The aim of the studies was to investigate an influence of tetrapropylammonium hydroxide (present in the leaching medium beside NaOH) and duration of desilication process on the catalytic performance of resulting micro-mesoporous Cu-ZSM-5. The obtained materials were tested in two environmental processes: selective catalytic reduction of NO with NH₃ and selective catalytic oxidation of NH₃.

2. Experimental methods

2.1. Catalysts preparation

The alkaline treatment of ZSM-5 (Si/Al~14, provided by Eka Chemicals) was performed using the solutions of sodium hydroxide (Chempur) and tetrapropylammonium hydroxide (TPAOH, Sigma-Aldrich). A first series of the samples was prepared using 100 mL of basic solution with

total concentration of OH⁻ equal to 0.2 M per 3.3 g of zeolite. The molar ratio of TPA⁺/OH⁻ in this series was equal to 0 (only NaOH was used) or 0.2. The resulting slurries were stirred under reflux at 65 °C for 1, 2, 4 or 6 h.

The obtained samples are denoted as follows: ZSM-5(TPA⁺/OH⁻ ratio equal 0.2 or nothing if only NaOH was used)/duration of desilication. Among this group of the samples, optimum desilication duration of 2 h was chosen. For this duration of desilication procedure an influence of the TPA⁺/OH⁻ ratio on the physicochemical properties of the samples was examined. We used the following molar TPA⁺/OH⁻ ratios: 0.2, 0.4, 0.6, 0.8 and ∞ (only TPAOH was used). This series of the samples was denoted as ZSM-5(TPA⁺/OH⁻ ratio)/2 h. All the sample codes and synthesis parameters are presented in Table 1.

Table 1. Synthesis parameters and textural properties of the samples determined from the N₂-sorption measurements.

Sample code	Leaching medium			TPA ⁺ /OH ⁻		Leaching duration/h			VMIC/cm ³ /g
	SMIC/m ² /g	VMES/cm ³ /g		SMES/m ² /g		SBET/m ² /g			
ZSM-5	–	–	–	0.157	356	0.078	96	389	
ZSM-5/1 h	NaOH	0	1	0.109	282	0.095	92	370	
ZSM-5(0.2)/1 h	NaOH/TPAOH	0.2	1	0.109	274	0.105	107	378	
ZSM-5/2 h	NaOH	0	2	0.058	161	0.226	190	377	
ZSM-5(0.2)/2 h	NaOH/TPAOH	0.2	2	0.079	188	0.222	224	427	
ZSM-5/4 h	NaOH	0	4	0.051	149	0.262	210	390	
ZSM-5(0.2)/4 h	NaOH/TPAOH	0.2	4	0.065	168	0.225	223	419	
ZSM-5/6 h	NaOH	0	6	0.018	75	0.537	446	453	
ZSM-5(0.2)/6 h	NaOH/TPAOH	0.2	6	0.053	143	0.244	239	416	
ZSM-5(0.4)/2 h	NaOH/TPAOH	0.4	2	0.089	220	0.167	187	399	
ZSM-5(0.6)/2 h	NaOH/TPAOH	0.6	2	0.106	252	0.144	165	398	
ZSM-5(0.8)/2 h	NaOH/TPAOH	0.8	2	0.118	281	0.123	144	398	
ZSM-5(∞)/2 h	TPAOH	1.0	2	0.149	354	0.063	82	384	

The Na-forms of the obtained samples (in order to convert them to H-forms) were triple exchanged with a 0.5 M solution of NH₄NO₃ (Sigma-Aldrich) at 80 °C for 1 h, filtered, washed with distilled water, dried at 60 °C and calcined at 600 °C for 6 h.

The subsequent copper exchange was carried out by immersing of zeolite in an aqueous solution of desired amount of Cu(CO₂CH₃)₂·H₂O (Sigma-Aldrich), with a zeolite/liquid ratio of

10 g/l and keeping under stirring at room temperature for 24 h. The concentration of the salt was adjusted to the aluminum content in the parent zeolite sample, taking into account the Cu/Al molar ratio of 0.5. Just before the end of the ion-exchange procedure, the 0.1 M solution of NH₄OH was added dropwise to increase pH of the slurry up to 6.5 (to prepare the samples with the copper content above the exchange capacity) [24,25].

2.2. Catalysts characterization

Textural properties of the samples were determined by N₂ sorption at -196 °C using a 3Flex v1.00 (Micromeritics) automated gas adsorption system. Prior to the analysis, the samples were degassed under vacuum at 350 °C for 24 h. The specific surface area (SBET) of the samples was determined using BET (Braunauer-Emmett-Teller) model according to Rouquerol et al. recommendations [26]. The micropore volume and specific surface area of micropores were calculated using the Harkins and Jura model (t-plot analysis, thickness range 0.55–0.85 nm). Mesopore volume and area were calculated from desorption branch using BJH model (Kruk-Jaroniec-Sayari empirical procedure) in the range of 1.7–30 nm. The pore size distributions were determined from the desorption branch of nitrogen isotherm by applying density functional theory (DFT). For calculations the method assuming nitrogen adsorption in cylindrical pores was used.

The X-ray diffraction (XRD) patterns of the samples were recorded using a Bruker D2 Phaser diffractometer. The measurements were performed in the 2 theta range of 5–50° with a step of 0.02°. The percentage crystallinity of the samples was estimated basing on the crystals sizes calculated using Scherrer's equation ($k = 1$, $\lambda = 0.154$ nm) for the reflection at 14.9°2 θ .

Surface acidity (concentration and strength of acid sites) of the samples was studied by temperature-programmed desorption of ammonia (NH₃-TPD). The measurements were performed in a flow microreactor system equipped with QMS detector (Prevac). Prior to ammonia sorption, a sample was outgassed in a flow of pure helium at 600 °C for 30 min. Subsequently, microreactor was cooled to 70 °C and the sample was saturated in a flow of gas mixture containing 1 vol% of NH₃ diluted in helium for about 120 min. Then, the catalyst was purged in a helium flow until a constant base line level was attained. Desorption was carried out with a linear heating rate (10 °C/min) in a flow of He (20 mL/min). Calibration of QMS with commercial mixtures allowed recalculating detector signal into the rate of NH₃ evolution.

Prior to the FTIR study the ZSM-5 sample was pressed into the form of self-supporting wafer (ca. 5 mg/cm²) and pre-treated in situ in quartz IR cell at 550 °C under vacuum conditions for 1 h. The IR spectra were recorded with a Bruker Tensor 27 spectrometer equipped with a MCT detector. The spectral resolution was 2 cm⁻¹. The concentration of Brønsted and Lewis acid sites was determined in quantitative IR studies of pyridine adsorption. The values of 0.10 cm²/μmol and 0.06 cm²/μmol were applied for the 1450 cm⁻¹ band of pyridine coordinatively bonded to Lewis sites (PyL) and for the 1545 cm⁻¹ band of pyridinium ions (PyH⁺), respectively. The acid strength was determined by pyridine thermodesorption experiments,

the intensity of the 1540 cm^{-1} (Brønsted sites) and 1450 cm^{-1} (Lewis sites) bands under desorption procedure at 500 °C was taken as a measure of the acid strength of the acid sites.

The transition metals content was analyzed by means of atomic absorption spectroscopy (Spectra AA 10 Plus, Varian).

Coordination and aggregation of transition metal species introduced into the obtained samples were studied by UV-vis-DR spectroscopy. The measurements were performed using an Evolution 600 (Thermo) spectrophotometer in the range of 200–900 nm with a resolution of 2 nm.

The reducibility of the samples was studied by temperature-programmed reduction with H₂ (H₂-TPR). Measurements were carried out in a quartz microreactor starting from room temperature up to 950 °C with a linear heating rate of 5 °C/min, using 5 vol% H₂ diluted in Ar (flow rate 5 mL/min). Before each measurement the samples (0.05 g) were purge in a flow of synthetic air (5 mL/min) and heated to 500 °C with heating rate of 10 °C/min. The hydrogen uptake was analyzed with the use of thermal conductivity detector (VICI, Valco instruments).

A Hitachi S-4700 scanning electron microscope equipped with a Thermo NSS system (for EDS microanalysis) was used to determine transition metal loadings in the calcined samples. Both secondary electrons (SE) and back-scattered electrons (YAG-BSE) detectors were used for imaging.

2.3. Catalytic tests

Catalytic studies of NH₃-SCR and NH₃-SCO were performed in a fixed-bed quartz microreactor. The experiments were done at atmospheric pressure and in the temperature range from 100 to 600 °C. The reactant concentrations were continuously measured using a quadrupole mass spectrometer (Prevac) connected directly to the reactor outlet. For each experiment 0.1 g of catalyst (particles sizes in the range of 0.160–0.315 mm) was placed on quartz wool plug in the reactor and outgassed in a flow of pure helium at 600 °C for 1 h. In case of the NH₃-SCR process the gas mixture containing 2500 ppm of NO, 2500 ppm of NH₃ and 25000 ppm of O₂ diluted in pure helium (total flow rate of 40 mL/min) was used. While in case of the NH₃-SCO process 5000 ppm of NH₃ and 25000 ppm of O₂ diluted in pure helium (total flow rate of 40 mL/min) was used.

3. Results and discussion

3.1. Characteristics of the as-synthesized samples

The intension of the undertaken studies was to modify the porous structure of the samples with the preservation of the zeolitic properties of ZSM-5. Thus, the effectiveness of the various desilication conditions applied was investigated by low-temperature N₂-sorption and XRD

measurements. The textural properties of the samples desilicated at different conditions measured by low-temperature N₂ sorption are presented in Table 1. Basic treatment of the samples resulted in significant changes in their textural properties. In the first series of the samples (TPA⁺/OH⁻ = 0 or 0.2), mesopore volume and mesopore surface area increased together with increasing duration of the desilication procedure. These changes in the textural characteristic of the samples proceeded in a favor of decrease in the micropore volume and micropore surface area. BET surface area of the samples did not change significantly and only slight increase in SBET for longer durations of alkaline treatment was observed. The samples desilicated at TPA⁺/OH⁻ = 0.2 are characterized by lower decrease in microporosity and greater development of mesoporosity in comparison to the samples treated only with NaOH. An exception in this tendency is the ZSM-5/6 h sample, for which the severe conditions strongly affected the micropore volume and micropore surface area.

In order to choose an optimal proportion between the generated mesoporosity and the loss of microporosity the hierarchy factor was analyzed [19]. Fig. 1 shows HF of the samples desilicated at TPA⁺/OH⁻ = 0 or 0.2, plotted as a function of the relative surface area of mesopores (SMES/STOT) and the relative micropore volume (VMIC/VTOT). The position of each sample in this graph defines its porous nature. In a bottom right corner the samples with a significant contribution of microporosity are located, while in a top left corner the samples with a significant contribution of mesoporosity can be find. Desilication of parent zeolite for 1 h resulted in a decrease in microporosity contribution (shift to the left side in relation to parent zeolite), however the contribution of mesoporosity did not change significantly. Prolongation of desilication duration to 2 and 4 h resulted in the further decrease in the relative micropore volume of the samples. But, in this case a significant development of mesoporosity (shift to the top) was observed. The outstanding sample, ZSM-5/6 h, desilicated at severe conditions (6 h, NaOH solution) is located in a top left corner, what proves its dominant mesoporous character. It is worth to notice that desilication at TPA⁺/OH⁻ = 0.2 is less dependent on duration of the desilication procedure in comparison to the samples treated only with NaOH. Moreover, the samples desilicated with addition of TPAOH are characterized by higher HF in comparison to the samples desilicated with NaOH. It proves the positive role of the pore directing agent (TPAOH), which preserves the microporous nature of the samples, simultaneously increasing their mesoporosity. Basing on the analysis of the results presented in Fig. 1 as the most effective desilication duration of 2 h was chosen. The ZSM-5/2 h and ZSM-5(0.2)/2 h samples are characterized by slightly higher HF in comparison to the samples desilicated for 4 h (HF calculated as (VMIC/VTOT) · (SMES/STOT)), what together with the lower preparation costs (shorter treatment time) points out 2 h as an optimum duration of the desilication process.

Fig. 1

[Download high-res image \(192KB\)](#)[Download full-size image](#)

Fig. 1. Hierarchy factor of the samples desilicated with TPA⁺/OH⁻ = 0 or 0.2 for different durations and reference ZSM-5, plotted as a function of the relative surface area of mesopores and the relative micropore volume.

Textural parameters of the second series of the samples (Table 1) prepared by 2 h of desilication using solutions with $\text{TPA}^+/\text{OH}^- = 0.2, 0.4, 0.6, 0.8$ or ∞ changed together with an increase in the amount of TPAOH used. Micropore volume and surface area increased, while mesoporosity decreased, reaching in the case of the ZSM-5(∞)/2 h sample values close to parent ZSM-5 zeolite. It proves that the leaching effectiveness of TPAOH is much weaker in comparison to NaOH. The changes in the micropore and mesopore volumes of the samples desilicated for 2 h with different TPA^+/OH^- ratio are presented in Fig. 2. The ZSM-5(0.2)/2 h sample is characterized by the highest mesopore volume among the samples in this series. Taking into account small differences in HF and decreased mesopore volume in the case of the other samples of this series the following parts of the studies were focused on the analysis of the samples desilicated at $\text{TPA}^+/\text{OH}^- = 0$ or 0.2 for different durations.

Fig. 2

[Download high-res image \(697KB\)](#)[Download full-size image](#)

Fig. 2. Changes in the micropore and mesopore volumes of the samples occurring after 2 h of desilication with the use of different TPA^+/OH^- ratio.

The nitrogen adsorption-desorption isotherms recorded for the samples desilicated for different durations using the bases mixture with the TPA^+/OH^- ratio equal to 0 or 2 and the reference microporous ZSM-5 are presented in Fig. 3. The shape of the isotherm recorded for reference ZSM-5 is of type I(a) (according to the IUPAC classification [27]) (Fig. 3(d)) and was changed after desilication for type IV(a), that proves generation of mesopores with diameter larger than 4 nm. 1 h of desilication resulted only in a slight development of mesoporosity, however the samples treated for a longer time are characterized by hysteresis loops typical of mesoporous materials. In case of the majority of the samples the shape of hysteresis loop can be classified as H4, characteristic of mesoporous zeolites with a broad distribution of mesopores sizes. Only in case of ZSM-5/6 h hysteresis loop can be assigned to H1 type, characteristic for materials with narrow distribution of uniform mesopores. The characteristic of mesopores obtained by the analysis of the nitrogen sorption isotherms can be confirmed by the DFT pore size distribution (Fig. 4). The mesopores generated in case of all the samples (besides ZSM-5/6 h) are in a wide range of pore sizes between about 4 and 18 nm. It is very important to notice that pore size distribution in case of the samples desilicated at $\text{TPA}^+/\text{OH}^- = 0.2$ is slightly narrower (about 4–13 nm) in comparison to the samples desilicated exclusively with NaOH. Similar observations were done by Sadowska et al. [21] for ZSM-5 desilicated with NaOH and NaOH/TBAOH mixtures. The treatment of zeolite with NaOH/TBAOH resulted in larger contribution of narrower mesopores, or mesopores penetrating zeolite crystals more deeply than for the samples treated only with NaOH. In case of the ZSM-5/6 h sample the microporosity was practically destroyed in a favor of developed mesoporosity, in a relatively narrow pore sizes range of 7–10 nm.

Fig. 3

[Download high-res image \(466KB\)](#)[Download full-size image](#)

Fig. 3. Nitrogen adsorption-desorption isotherms of the samples desilicated with TPA+/OH⁻ = 0 or 0.2 for 1(a), 2(b), 4(c) and 6(d) h.

Fig. 4

[Download high-res image \(396KB\)](#)[Download full-size image](#)

Fig. 4. Pore size distributions calculated by DFT method for the samples desilicated with TPA+/OH⁻ = 0 or 0.2 for different durations and reference ZSM-5.

The XRD powder patterns of the samples desilicated with a mixture of TPA+/OH⁻ = 0 or 0.2 for different durations and reference parent ZSM-5 are presented in Fig. 5(a). In all cases the reflections characteristic of the MFI structure type were found [28,29]. It proves that during desilication (even under the more severe conditions) the zeolitic character of the samples was maintained. The intensity of the XRD reflections decreased together with an increase of desilication duration. However, any significant crystallographic differences between the samples desilicated with TPA+/OH⁻ mixture or exclusively with NaOH were observed. The changes in the samples crystallinity were estimated basing on the crystal sizes determined by Schererr's equation ($k = 1$, $\lambda = 0.154$ nm, reflection at $14.9^{\circ}2\theta$) and are presented in Table 2. The crystals sizes decreased after desilication process together with an increase of alkaline treatment duration. To evaluate the changes in the samples crystallinity occurring during their modifications it was assumed that the parent ZSM-5 sample is crystalline in 100%. One hour of desilication did not influence significantly the samples crystallinity, while extended alkaline treatment resulted in partial amorphisation of the zeolite samples (30–50%). It is worth to mention that the treatment with bases mixture (TPA+/OH⁻ = 0.2) decreased the samples crystallinity more effectively than in the case of the use of exclusively NaOH (the results are in agreement with N₂-sorption results).

Fig. 5

[Download high-res image \(658KB\)](#)[Download full-size image](#)

Fig. 5. XRD diffraction patterns of the samples desilicated for different durations with TPA+/OH⁻ = 0 or 0.2 and reference ZSM-5 before (a) and after modification with Cu (b).

Table 2. Surface concentration of acid sites (CA) measured by NH₃-TPD; changes in the samples crystallinity determined by XRD and Cu, Si and Al content measured by AAS analysis.

Sample code Cu/Al	CA/ $\mu\text{mol/g}$	Crystallinity/%	Sample code	CA/ $\mu\text{mol/g}$	Si/Al	Cu/%
ZSM-5 292	100	Cu-ZSM-5 330	14	1.2	0.18	
ZSM-5/1 h	414	99	Cu-ZSM-5/1 h 468	13	2.8	0.43
ZSM-5(0.2)/1 h	413	99	Cu-ZSM-5(0.2)/1 h 470	13	2.5	0.48
ZSM-5/2 h	469	75	Cu-ZSM-5/2 h 550	10	3.9	0.45
ZSM-5(0.2)/2 h	441	64	Cu-ZSM-5(0.2)/2 h 609	10	3.8	0.48
ZSM-5/4 h	519	62	Cu-ZSM-5/4 h 561	10	3.8	0.39
ZSM-5(0.2)/4 h	530	60	Cu-ZSM-5(0.2)/4 h 535	10	3.7	0.47
ZSM-5/6 h	489	61	Cu-ZSM-5/6 h 542	10	4.1	0.48
ZSM-5(0.2)/6 h	493	58	Cu-ZSM-5(0.2)/6 h 575	10	3.8	0.47

Another important factor for the catalytic application, which can be tuned by desilication is surface acidity of the samples. Surface concentration of acid sites (CA) in the samples measured by temperature-programmed desorption of ammonia (NH₃-TPD) is presented in Table 2. The values of CA were calculated by integration of the areas under TPD profiles, which were recalculated into a number of adsorbed ammonia molecules (it was assumed that one NH₃ molecule adsorbs on one acid site). Surface concentration of acid sites, equals to 292 $\mu\text{mol/g}$ in the case of parent ZSM-5, significantly increased after desilication. Even after the shortest time of desilication (1 h) the concentration of acid sites increased by about 30%. This increase was observed up to 4 h of alkaline treatment. However, this trend changed after 6 h and the values of CA decreased. An increase in surface concentration of acid sites during first hours of desilication can be correlated to the increase in relative Al content caused by a partial silicon extraction [30]. Prolongation of alkaline treatment to 6 h resulted in a decrease of CA, what can be connected with the extraction (beside Si) of framework Al to the extra-framework positions [31]. The changes in surface acidity, observed after desilication, are in agreement with the changes in the Si/Al ratio measured by AAS technique (Table 2) Alkaline treatment of the samples resulted in a decrease of the Si/Al ratio from 14 to 13 after 1 h and to 10 after 2 h. Further prolongation of desilication duration did not affect the ratio of silica and alumina contents in the samples (what could be connected with the simultaneous Al extraction and/or its deposition on the catalysts surface).

It is worth to notice that the values of the concentration of acid sites measured by NH₃-TPD and the Si/Al ratio measured by AAS technique are not complementary. The surface concentration of acid sites determined for the parent ZSM-5 sample, which is 292 $\mu\text{mol/g}$, is equivalent to the Si/Al ratio of about 56, while the value determined by ASS analysis is 14. This difference results from the presence of non-acidic aluminium species in parent ZSM-5 supplied by Eka Chemicals. The IR spectra recorded for parent ZSM-5 in the region of the OH stretching vibrations providing information about the acidic properties is presented in Fig. 6. In this spectra four bands of hydroxyls differing in acidity can be distinguished, at about 3740, 3710, 3660 and 3610 cm^{-1} . They can be assigned respectively to the vibrations of isolated Si-OH

silanols located at the external surface, vicinal (bonded by hydrogen bonding to the framework oxygen), Si-OH silanols at the crystal defects, Al-OH non-acidic groups and Si(OH)Al strong acidic bridging groups [32]. The high intensity of the band at about 3660 cm^{-1} proved the presence of non-acidic aluminium (possibly also extraframework) in the parent ZSM-5 sample, what explained the differences between the sample acidity and the content of aluminum.

Fig. 6

[Download high-res image \(231KB\)](#)[Download full-size image](#)

Fig. 6. IR spectra in OH vibrations region recorded for parent ZSM-5 material.

In all the obtained desorption profiles (Fig. 7) two desorption peaks, corresponding to weak acid sites at about 210 °C (so called α sites) and to strong acid sites around 400 °C (so called γ sites), can be distinguished [33]. The shape of ammonia desorption profiles did not change significantly after desilication at different conditions. However, a slight shift of the peak at about 210 °C to the higher temperatures was observed. Such shift indicates the presence of slightly stronger acid sites in the mesostructured samples. In order to analyze the nature of acid sites more deeply, the acidic properties of parent ZSM-5 were studied by pyridine sorption. Total concentration of acid sites measured by Py-sorption was equal to 267 $\mu\text{mol/g}$ (173 $\mu\text{mol/g}$ Brønsted sites, 94 $\mu\text{mol/g}$ Lewis sites). Slightly higher value obtained by NH_3 sorption can be connected with smaller dimension of ammonia molecule in comparison to pyridine what enabled better penetration of zeolite crystals. The concentration of Brønsted acid sites, related to the presence of tetrahedral coordinated aluminum, is higher than concentration of Lewis acid sites. Thus, they can be related to α and γ acid sites detected by NH_3 -TPD, respectively. The strength of acid sites expressed as a ratio of 1540 cm^{-1} (Brønsted sites) and 1450 cm^{-1} (Lewis sites) bands intensities at room temperature and after desorption at 500 °C ($A_{500^\circ\text{C}}/A_0$) was equal to 0.54 and 0.47, respectively. This relatively weak strength of acid sites (usually for ZSM-5 zeolite this ratio is close to 1 [34]) can be connected with the presence of significant amount of non-acidic aluminum in the parent material.

3.2. Characteristics of the Cu-modified samples

Since the presence of red-ox active sites plays an important role in both the studied catalytic processes (selective catalytic reduction of NO with NH_3 and selective catalytic oxidation of NH_3) the obtained samples were modified with Cu by ion-exchange method. It is important to notice that the modification procedure did not influence the crystalline structure of the samples, what was verified by the X-ray diffraction method (Fig. 5(b)). The Cu-modified samples were analyzed with respect to the content (AAS analysis, Table 2) and form of the introduced metal species (UV-vis-DR spectroscopy and temperature programmed reduction with H_2 (H_2 -TPR), Figs. 8 and 9 respectively). The copper content in the samples, considering that the same modification procedure was applied in case of all the samples (ion-exchange), differ depending on the duration of desilication. 1 h of alkaline treatment resulted in an increase of Cu content from about 1 wt% to 3 wt%, while 2 h to 4 wt%, approximately. Further

prolongation of desilication duration did not influence significantly the content of introduced metal and its content maintained at about 4 wt%. An increase in Cu content caused by desilication can be connected with the better accessibility of ion-exchange positions in mesoporous zeolite and increased surface acidity of the samples. The Cu/Al ratio determined by AAS technique is close to 0.5 (100% of IE calculated basing on Si/Al) in case of the micro-mesoporous samples, while is much lower for the parent ZSM-5 sample. What proved that the micro-mesoporous structure of the samples enabled introduction of greater amount of transition metal with the same method used. It should also be noticed that much greater amount of copper (above IE capacity) was introduced to the samples in relation to the concentration of acid sites (corresponding to Brønsted exchangeable H⁺ sites). This phenomenon occurred as a result of the applied so-called excess ion exchange procedure. Although the Cu/Al ratio measured by AAS is below 0.5, a significant amount of Al in the samples was identified as non-acidic (Fig. 6) what means that the samples are Cu-overloaded. Such preparation method (with the use of NH₄OH at the end of the ion-exchange procedure) enables enrichment of the catalyst surface with well dispersed copper (better distribution of transition metal across the zeolite crystal in comparison to the impregnated samples), which is easily reducible to copper (I) [35,36]. Cu-ZSM-5 with high Cu loadings and over-exchanged is considered in the literature as the most active in the SCR reactions [35–38].

Fig. 7

[Download high-res image \(408KB\)](#)[Download full-size image](#)

Fig. 7. NH₃-TPD profiles of the samples desilicated for different durations with TPA⁺/OH⁻ = 0 or 0.2 and reference ZSM-5. Conditions: 10000 ppm NH₃ in He; gas flow 20 mL/min; weight of catalyst - 0.05 g.

Fig. 8

[Download high-res image \(401KB\)](#)[Download full-size image](#)

Fig. 8. UV-vis-DR spectra of the samples desilicated with TPA⁺/OH⁻ = 0 or 0.2 for 1(a), 2(b), 4(c) and 6(d) h.

Fig. 9

[Download high-res image \(466KB\)](#)[Download full-size image](#)

Fig. 9. H₂-TPR profiles of the samples desilicated for different durations with TPA⁺/OH⁻ = 0 or 0.2 and reference ZSM-5. Conditions: 50000 ppm H₂ in Ar; gas flow 5 mL/min; weight of sample - 0.05 g.

The concentration of acid sites in the samples modified with copper is presented in Table 2. In the case of all the samples the surface acidity increased after introduction of transition metal. The shape of ammonia desorption profiles obtained in the case of the Cu-samples differs from their H-forms (results not shown). The separated band observed in the case of the H-samples (Fig. 7) at about 400 °C, connected with the presence of the strong Brønsted acid sites significantly decreased and was shifted to lower temperatures. The observed changes are connected with the replacement of exchangeable protons by copper cations, which are acid centers of Lewis type. An increase in total concentration of acid sites can be explained by higher Cu content in comparison to ion-exchange capacity of zeolite. Introduced copper occupied not only the ion-exchange positions but also formed small oligomeric or bulky CuO species on the samples surface. Similar observations were done in the previous studies concerning Cu-modified MCM-22 zeolite [18]. The highest values (also the highest increase in acidity) of CA were obtained for the samples desilicated for 2 h, which, as it was shown by AAS measurements, were loaded with the highest Cu content (the highest Cu/Al ratio).

Fig. 8 shows the UV-vis-DR spectra of the samples desilicated for different durations using the bases mixture with the TPA⁺/OH⁻ ratio equal to 0 or 2, being compared with reference microporous ZSM-5. In case of all the samples two distinct peaks at about 250 nm (the sharp one) and 700 nm (the broad one) were obtained. The absorption bands at about 200–300 nm can be assigned to oxygen-to-metal charge transfer related to Cu⁺ or Cu²⁺ cations (centered respectively at about 210 and 250 nm) stabilized by the zeolite framework [39–41]. Some works [42,43] attribute the band at about 210 nm to the zeolite structure (band originating from the charge transfer O²⁻—Al³⁺) and the bands at higher wavelengths to Cu⁺ and Cu²⁺ (centered at about 250 and 300 nm, respectively). However, independently from the exact assignment (the band originated from the zeolite structure can overlap with the bands characteristic of MLCT) it can be concluded that this absorption range is related to copper introduced to ion-exchange positions. Copper was introduced in the form of divalent cations, however part of Cu could undergo reduction during calcination and the presence of Cu⁺ cannot be excluded. The absorption in the range 600–900 nm is related to d-d transitions of Cu²⁺ in octahedral oxygen coordination, more or less tetragonally distorted, which can be attributed to dispersed surface CuO particles [39,44]. Gang et al. [45] related the absorption in this range to the presence of CuO (maximum at about 650 nm) and CuAl₂O₄ or [Cu-O-Cu]₂⁺ (maximum at about 750 nm). The presence of all these forms of copper can be connected with the overloading of the samples with Cu and the presence of significant amount of non-acidic (possibly extra-framework) aluminum. However, the dispersion of such Cu species is probably very high, what did not enable their detection by XRD (Fig. 5(b)). The lack of any bands in the range of 300–600 nm proved the absence of oligomeric Cu²⁺—O²⁻—Cu²⁺ chains (expected at about 300–400 nm) and metallic copper Cu⁰ (about 570 nm) in the samples [44,46,47].

Basing on the UV-vis-DRS results, it can be concluded that copper was introduced to both types of materials (microporous and micro-mesoporous) in similar forms (monomeric cations stabilized by the zeolite framework and small oxide or aluminate forms dispersed on the zeolite surface). The band at about 200–300 nm obtained for the parent ZSM-5 sample is slightly shifted to lower wavelengths what could be attributed to slightly higher contribution of Cu⁺ in this sample. However, it has to be stressed that this band is still in the spectral range

characteristic of both Cu⁺ and Cu²⁺. The duration of alkaline leaching and the TPA⁺/OH⁻ ratio did not influence the Cu form in the samples.

The results of temperature programmed reduction of the samples with H₂ are presented in Fig. 9. In the case of the parent ZSM-5 sample the reduction profile consists of three reduction steps which can be attributed to Cu²⁺ → Cu⁺ (Cu²⁺ + ½ H₂ → Cu⁺ + H⁺), CuO → Cu⁰ (Cu²⁺ + H₂ → Cu⁰ + 2H⁺) and Cu⁺ → Cu⁰ (Cu⁺ + ½ H₂ → Cu⁰ + H⁺), respectively [48–51]. In the case of the micro-mesoporous samples only two reduction steps (Cu²⁺ → Cu⁺ and Cu⁺ → Cu⁰) were observed. It proved that in case of conventional zeolite Cu²⁺ in octahedral oxygen coordination identified by UV-vis-DR spectroscopy had stronger tendency towards formation of CuO on the catalyst surface. It is important to notice that the reduction of copper introduced to the alkaline treated samples proceeds at lower temperatures in comparison to parent ZSM-5. The shift of these bands to lower temperatures proved better reducibility of copper present in the micro-mesoporous samples, what could be connected with weaker stabilization of copper oxidation state by defected zeolite lattice or improved copper exposure by the generated mesoporosity.

The small and broad reduction peak at about 100 °C, visible especially in the reduction profiles of the micro-mesoporous samples, could be assigned to [Cu-O-Cu]₂²⁺ dimeric cations reduction to Cu⁺[52], however a straight assignment of the band at that low temperature should be very careful.

Deconvolution of the reduction profiles into sub-bands enabled estimation of the percentage contribution of the particular Cu forms in the samples (band at 100 °C was not taken into account) (Table 3). The content of Cu²⁺ and CuO was calculated basing on the surface area of the reduction profiles at about 280–290 °C and 400 °C, respectively. While the contribution of Cu⁺ was calculated as a difference between the reduction bands Cu²⁺ → Cu⁺ and Cu⁺ → Cu⁰. Divalent copper species introduced to the modified, micro-mesoporous samples are much more easy reducible to Cu⁺ and stabilized by the zeolite structure. Despite degassing of the samples in the air atmosphere before H₂ reduction a significant amount of copper was present in monovalent form (in case of the samples desilicated for 2 h about 50%). It is worth to notice that the content of Cu⁺ present in the samples treated with the NaOH/TPAOH mixture is slightly higher. However, due to the asymmetry of the reduction bands the obtained values must be treated as estimations.

Table 3. Estimation of the percentage content of different Cu forms in the samples basing on the H₂ consumption.

Sample code	Cu ²⁺ /%	Cu ⁺ /%	CuO/%
ZSM-5 44	–	56	
ZSM-5/1 h	100	–	–
ZSM-5(0.2)/1 h 99	1	–	

ZSM-5/2 h	54	46	–
ZSM-5(0.2)/2 h	40	60	–
ZSM-5/4 h	69	31	–
ZSM-5(0.2)/4 h	67	32	–
ZSM-5/6 h	83	17	–
ZSM-5(0.2)/6 h	66	34	–

The changes in the samples morphology occurring during desilication and modification with copper are presented for the chosen samples: ZSM-5, ZSM-5/2 h and ZSM-5(0.2)/2 h (before and after modification with Cu) in Fig. 10. The crystals of parent zeolite are characterized by sharp edges and regular form typical of ZSM-5 [53]. After desilication, both with the use of the TPA⁺/OH⁻ ratio equal to 0 or 2, the morphology of crystals significantly changed. Partial dissolution of the samples resulted in a cauliflower-like loose structure with rounded edges crystals, what is especially visible when NaOH/TPAOH mixture was used as desilication agent (the ZSM-5(0.2)/2 h sample). The observed changes are in agreement with the development of the textural parameters determined by N₂-sorption (Table 1). The BET surface area and the surface of mesopores were larger in the case of ZSM-5(0.2)/2 h in comparison to ZSM-5/2 h. After modification with Cu the morphology of the samples did not change significantly. The analysis of the samples with EDS (X-ray energy dispersive spectrometry) and BSE (back-scattered electron) detectors enabled the study of copper distribution on the surface of the samples. In the case of Cu-ZSM-5 small regions of higher copper concentration were found (white spots in Fig. 11). The Cu concentration measured in point 1 was equal to about 15 wt%, while in point 2 was about 1 wt%. In the case of the desilicated samples no regions of higher copper aggregation were found and the Cu concentration measured in different locations by EDS was in the range of about 3–4 wt%, what is in agreement with the results of ICP, H₂-TPR and UV-vis-DRS measurements.

Fig. 10

[Download high-res image \(536KB\)](#)[Download full-size image](#)

Fig. 10. SEM micrographs (secondary electrons) of the parent ZSM-5 zeolite and the samples desilicated for 2 h with TPA⁺/OH⁻ = 0 or 0.2 before (a) and after modification with Cu (b).

Fig. 11

[Download high-res image \(230KB\)](#)[Download full-size image](#)

Fig. 11. SEM micrograph (back-scattered electrons) of the Cu-ZSM-5 sample.

3.3. Catalytic study: NH₃-SCR and NH₃-SCO

The results of the catalytic tests of the samples desilicated for different durations at TPA⁺/OH⁻ = 0 (only NaOH was used) and reference parent ZSM-5 in the DeNO_x process are presented in Fig. 12. The catalytic activity of the samples significantly increased after their treatment with NaOH. The order of the catalytic activity of the micro-mesoporous samples presents as follows: Cu-ZSM-5/2 h > Cu-ZSM-5/4 h > Cu-ZSM-5/1 h > Cu-ZSM-5/6 h > Cu-ZSM-5. The obtained activity order is neither in a straight relation with the samples surface acidity nor with the copper content.

Fig. 12

[Download high-res image \(362KB\)](#)[Download full-size image](#)

Fig. 12. Temperature dependence of NO conversion and N₂ selectivity in SCR of NO with NH₃ for the samples desilicated for different durations with TPA⁺/OH⁻ = 0 and the reference parent ZSM-5. Conditions: 2500 ppm NO, 2500 ppm NH₃, 25000 ppm O₂; He as balancing gas; total flow rate - 40 mL/min; weight of catalyst - 0.1 g.

In order to compare the catalytic activity of the samples independent from the metal content and the specific surface area (the samples significantly differ in the copper content) the calculations of turnover frequency (TOF) were performed (Table 4) [54,55]. The calculations were done with assumption that each Cu atom (AAS measurements) acts as an active center. The efficiency of the active sites in the samples after modification significantly differs from the conventional ZSM-5. Copper centers with the highest activity were identified in the sample desilicated for 1 h. Together with an increase of the alkaline treatment the TOF values decrease and for the sample desilicated for 6 h reaches value similar to the reference sample. Thus, it seems that the significantly higher NO conversion over the micro-mesoporous samples can be connected with the interaction of complex factors including the content of copper species and their improved reducibility, increased acidity and the hierarchy factor of the samples, what points out the benefits of alkaline pre-treatment of the samples in case of this reaction. Moreover, it is important to notice that the divalent copper present in the micro-mesoporous samples is easily reduced to Cu⁺ and stabilized in the zeolite structure. In agreement with the previous findings the samples with the facile conversion between Cu²⁺ and Cu⁺ were found as the most active in the SCR process [e.g. 36, 37].

Table 4. TOF (turnover frequency) defined as the number of NO or NH₃ molecules converted over the individual Cu site per second in NH₃-SCR and NH₃-SCO processes, respectively.

TOF 10 ⁻³ /s ⁻¹	Cu-ZSM-5	Cu-ZSM-5/1 h	Cu-ZSM-5/2 h	Cu-ZSM-5/4 h	Cu-ZSM-5/6 h
NH ₃ -SCR (225 °C)	0.54	1.36	1.04	1.02	0.76
NH ₃ -SCO (350 °C)	1.55	2.40	2.05	1.97	1.55

In the case of all the studied samples, a sharp drop in the NO conversion was observed at about 375 °C. This phenomenon is connected with a side, competitive process of direct ammonia oxidation that typically became more significant at high temperatures. It is worth to notice that the samples alkaline treated for 1, 2 and 4 h are more active in the side process of direct ammonia oxidation in comparison to parent ZSM-5, what decreased their efficiency in the high-temperature DeNO_x process. On the other hand, such results may suggest high catalytic activity of alkaline treated zeolites in the process of selective ammonia oxidation to nitrogen. This concept is supported by high selectivity to N₂ in the case of all the samples, which did not drop below 90% (in the examined temperature range of high conversion) (Fig. 12).

The comparison of the catalytic activity in the DeNO_x process of the samples desilicated with the bases mixture at TPA⁺/OH⁻ ratio equal to 0.2 with the samples desilicated exclusively with NaOH is presented as temperature necessary to obtain 50% of NO conversion (T₅₀) in Fig. 13. In the case of the desilicated samples the temperature of 50% conversion was significantly lower in comparison to parent ZSM-5. The difference between the samples desilicated with NaOH/TPAOH mixture and only with NaOH is clearly visible up to 2 h of treatment and the samples modified with the use of pore directing agent (TPAOH) showed higher catalytic activity (lower T₅₀). Further prolongation of desilication duration decreased the difference between the used alkaline solutions and finally after 6 h the Cu-ZSM-5(DS)/6 h sample showed lower T₅₀. These changes can be connected with the weaker desilication efficiency with increasing treatment duration with TPAOH in comparison to pure NaOH (weaker dependency of alkaline treatment duration), what was also reflected in the presented above physicochemical properties of the samples. Selectivity of the reaction to N₂ in case of the samples treated with the mixture of NaOH and TPAOH (results not shown) did not differ significantly from the selectivity obtained for the samples treated exclusively with NaOH and was maintained above 90% for all the samples.

Fig. 13

[Download high-res image \(846KB\)](#)[Download full-size image](#)

Fig. 13. Temperature of 50% conversion of the samples desilicated for different durations with TPA⁺/OH⁻ = 0 or 0.2 and reference ZSM-5 in DeNO_x process.

The results of selective catalytic oxidation of ammonia over the samples desilicated for different durations at TPA⁺/OH⁻ = 0 (only NaOH was used) and over reference Cu-ZSM-5 are presented in Fig. 14. Similarly to DeNO_x a significant increase of ammonia conversion was observed over the modified, micro-mesoporous samples. Moreover, also the same order of the catalytic activity of the samples (Cu-ZSM-5/2 h > Cu-ZSM-5/4 h > Cu-ZSM-5/1 h > Cu-ZSM-5/6 h > Cu-ZSM-5) as in case of the DeNO_x process was observed, pointing out that the copper species with the best reducibility are the most active species in the process of selective ammonia oxidation. Also the values of TOF (Table 3), independent from the copper content in the samples, indicate the higher catalytic activity of the active sites present in the micro-

mesoporous samples. Thus, similarly to NH₃-SCR, the improved catalytic efficiency of the desilicated samples in ammonia oxidation can be explained as a result of easier reducibility of copper species in such defected systems. The selectivity of the NH₃-SCO process to nitrogen was maintained above 90% in the examined temperature range of high conversion (>80%).

Fig. 14

[Download high-res image \(328KB\)](#)[Download full-size image](#)

Fig. 14. Temperature dependence of NH₃ conversion and N₂ selectivity in SCO of NH₃ for the samples desilicated for different durations with TPA⁺/OH⁻ = 0 and the reference parent ZSM-5. Conditions: 5000 ppm NH₃, 25000 ppm O₂; He as balancing gas; total flow rate - 40 mL/min; weight of catalyst - 0.1 g.

The comparison of T50 for the samples desilicated with NaOH and NaOH/TPAOH mixture in NH₃-SCO is presented in Fig. 15. In case of ammonia oxidation only slight difference between these two series of the catalysts was observed. The alkaline treatment of the zeolite for 1, 2 and 4 h with NaOH resulted in a decrease of T50 (in comparison to the series treated with NaOH/TPAOH mixture), while the catalysts obtained from zeolite treated for 6 h with NaOH (Cu-ZSM-5(0.2)/6 h) presented lower activity (what can be connected with the stronger desilication effect of NaOH). Also, in the case of the samples treated with the mixture of NaOH and TPAOH the selectivity to nitrogen was maintained above 90% (results not shown).

Fig. 15

[Download high-res image \(933KB\)](#)[Download full-size image](#)

Fig. 15. Temperature of 50% conversion of the samples desilicated for different durations with TPA⁺/OH⁻ = 0 or 0.2 and reference ZSM-5 in NH₃-SCO process.

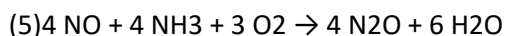
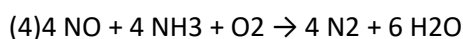
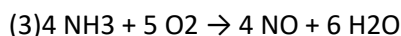
The comparison of NO and NH₃ conversion in the NH₃-SCR and NH₃-SCO processes, respectively, over the most active catalysts (Cu-ZSM-5/1 h, Cu-ZSM-5(0.2)/1 h, Cu-ZSM-5/2 h and Cu-ZSM-5(0.2)/2 h) is presented in Fig. 16. In the case of all the samples the low temperature conversion of NO is favorable. At higher temperatures a sharp drop in NO conversion that corresponds with the maximum of NH₃ conversion in NH₃-SCO is observed. This result confirms the preferable conditions for the studied reaction above 400 °C.

Fig. 16

[Download high-res image \(590KB\)](#)[Download full-size image](#)

Fig. 16. Comparison of NO and NH₃ conversion in the NH₃-SCR and NH₃-SCO processes over the Cu-ZSM-5/1 h, Cu-ZSM-5(0.2)/1 h, Cu-ZSM-5/2 h and Cu-ZSM-5(0.2)/2 h samples.

The observed phenomenon can be explained by so called internal SCR mechanism (i-SCR). According to this mechanism in the first step ammonia is oxidized to NO, while in the second step the unreacted ammonia reduces NO to N₂ or N₂O (Eqs. (3)–(5)):



Ammonia oxidation is a rate determining step of this reaction and therefore at low temperatures ammonia plays a role of NO reducer in NH₃-SCR, while at higher temperatures it starts to be oxidized by oxygen present in the reaction mixture. This mechanism was earlier observed for other groups of catalytic materials e.g. Cu-containing hydrotalcites (Chmielarz et al. [4, 56]) or mesoporous Fe-modified ZSM-5 obtained by desilication and direct synthesis (Góra-Marek et al. [13]). A schematic representation of the described above mechanism is presented in Fig. 17.

Fig. 17

[Download high-res image \(234KB\)](#)[Download full-size image](#)

Fig. 17. Schematic representation of the i-SCR mechanism.

4. Conclusions

Modification of ZSM-5 zeolite by desilication with NaOH and NaOH/TPAOH mixture resulted in generation of mesoporosity with simultaneous decrease in micropore volume and crystallinity of the samples and increase in the surface acidity. The best ratio between the generated mesoporosity and the loss in microporosity was obtained with the use of bases mixture at TPA⁺/OH⁻ = 0.2 and desilication duration of 2 h (the ZSM-5(0.2)/2 h sample). The applied modifications resulted in introduction (by ion-exchange) of different amount of copper with various reducibility properties. Improved reducibility of Cu species is most probably responsible for the enhanced catalytic activity of the micro-mesoporous samples in the NH₃-SCR and NH₃-SCO processes. Moreover, divalent Cu introduced to the micro-mesoporous samples was easily reduced to Cu⁺. Concluding, modification of micro-mesoporous zeolites by desilication enable tuning of the porous structure, acidity and red-ox properties of introduced metals, improves the properties of classical zeolites and makes them very promising group of materials for the future more detailed studies focused on their application in catalysis.

Acknowledgements

This work was supported by the National Science Center under grant no. 2011/03/N/ST5/04820. Part of the research was carried out with the equipment purchased thanks to the financial support of the European Regional Development Fund in the framework of the Polish Innovation Economy Operational Program (contract no. POIG.02.01.00-12-023/08). U. D. acknowledges to Spanish Government by the funding (MAT2014-52085-C2-1-P).

References

[1]

P. Granger, V.I. Parvulescu
Chem. Rev., 111 (2011), pp. 3155-3207
CrossRefView Record in Scopus

[2]

L. Ma, Y. Cheng, G. Cavataio, R.W. McCabe, L. Fu, J. Li
Chem. Eng. J., 225 (2013), pp. 323-330
ArticleDownload PDFView Record in Scopus

[3]

B. Guan, R. Zhan, H. Lin, Z. Huang
Appl. Therm. Eng., 66 (2014), pp. 395-414
ArticleDownload PDFView Record in Scopus

[4]

L. Chmielarz, M. Jabłońska
RSC Adv., 54 (2015), pp. 43408-43431
CrossRefView Record in Scopus

[5]

L. Zhang, J. Pierce, V.L. Leung, D. Wang, W.S. Epling
J. Phys. Chem. C, 117 (2013), pp. 8282-8289
CrossRefView Record in Scopus

[6]

S. Yashnik, Z. Ismagilov
Appl. Catal. B Environ., 170–171 (2015), pp. 241-254
ArticleDownload PDFView Record in Scopus

[7]

N. Wilken, K. Wijayanti, K. Kamasamudram, N.W. Currier, R. Vedaiyan, A. Yezerets, L. Olsson
Appl. Catal. B Environ., 111–112 (2012), pp. 58-66

[ArticleDownload](#) [PDFView](#) [Record in Scopus](#)

[8]

D.W. Fickel, E. D'Addio, J.A. Lauterbach, R.F. Lobo
Appl. Catal. B Environ., 102 (2011), pp. 441-448

[ArticleDownload](#) [PDFView](#) [Record in Scopus](#)

[9]

M. Valdez Lancinha Pereira, A. Nicolle, D. Berthout
Catal. Today, 258 (2015), pp. 424-431

[ArticleDownload](#) [PDFView](#) [Record in Scopus](#)

[10]

D.P. Serrano, J.M. Escola, P. Pizarro
Chem. Soc. Rev., 42 (2013), pp. 4004-4035

[CrossRefView](#) [Record in Scopus](#)

[11]

R. Chal, C. Gérardin, M. Bulut, S. van Donk
ChemCatChem, 3 (2011), pp. 67-81

[CrossRefView](#) [Record in Scopus](#)

[12]

M.S. Holm, E. Taarning, K. Egeblad, C.H. Christensen
Cat. Today, 168 (2011), pp. 3-16

[ArticleDownload](#) [PDFView](#) [Record in Scopus](#)

[13]

K. Góra-Marek, K. Brylewska, K.A. Tarach, M. Rutkowska, M. Jabłońska, M. Choi, L. Chmielarz
Appl. Catal. B Environ., 179 (2015), pp. 589-598

[ArticleDownload](#) [PDFView](#) [Record in Scopus](#)

[14]

Y. Yue, H. Liu, P. Yuan, C. Yu, X. Bao
Sci. Rep., 5(9270) (2015), pp. 1-10, 10.1038/srep09270

[View](#) [Record in Scopus](#)

[15]

J. Ma, D. Weng, X. Wu, Z. Si, Z. Wu
Prog. Nat. Sci. Mat. Int., 23 (5) (2013), pp. 493-500
ArticleDownload PDFView Record in Scopus

[16]

P.N.R. Vennestrøm, M. Grill, M. Kustova, K. Egeblad, L.F. Lundegaard, F. Joensen, C.H. Christensen, P. Beato
Catal. Today, 168 (2011), pp. 71-79
ArticleDownload PDFView Record in Scopus

[17]

A.L. Kustov, T.W. Hansen, M. Kustova, C.H. Christensen
Appl. Catal. B Environ., 76 (2007), pp. 311-319
ArticleDownload PDFView Record in Scopus

[18]

M. Rutkowska, U. Díaz, A.E. Palomares, L. Chmielarz
Appl. Catal. B Environ., 168 (2015), pp. 531-539
ArticleDownload PDFView Record in Scopus

[19]

J. Pérez-Ramírez, D. Verboekend, A. Bonilla, S. Abelló
Adv. Funct. Mater., 19 (2009), pp. 3972-3979
View Record in Scopus

[20]

D. Verboekend, G. Vilé, J. Pérez-Ramírez
Cryst. Growth Des., 12 (6) (2012), pp. 3123-3132
CrossRefView Record in Scopus

[21]

K. Sadowska, A. Wach, Z. Olejniczak, P. Kuśtrowski, J. Datka
Microporous Mesoporous Mater., 167 (2013), pp. 82-88
ArticleDownload PDFView Record in Scopus

[22]

K. Sadowska, K. Góra-Marek, M. Drozdek, P. Kuśtrowski, J. Datka, J. Martinez Triguero, F. Rey

Microporous Mesoporous Mater., 168 (2013), pp. 195-205

[ArticleDownload](#) [PDFView](#) [Record in Scopus](#)

[23]

K. Sadowska, K. Góra-Marek, J. Datka

Vib. Spectrosc., 63 (2012), pp. 418-425

[ArticleDownload](#) [PDFView](#) [Record in Scopus](#)

[24]

A.E. Palomares, F. Márquez, S. Valencia, A. Corma

J. Mol. Catal. A Chem., 162 (2000), pp. 175-189

[ArticleDownload](#) [PDFView](#) [Record in Scopus](#)

[25]

A. Corma, V. Fornés, E. Palomares

Appl. Catal. B Environ., 11 (1997), pp. 233-242

[ArticleDownload](#) [PDFView](#) [Record in Scopus](#)

[26]

J. Rouquerol, P. Llewellyn, F. Rouquerol

Stud. Surf. Sci. Catal., 160 (2007), p. 49

[ArticleDownload](#) [PDFView](#) [Record in Scopus](#)

[27]

M. Thommes, K. Kaneko, A.V. Neimark, J.P. Olivier, F. Rodriguez-Reinoso, J. Rouquerol, K.S.W. Sing

Pure Appl. Chem., 87 (9–10) (2015), pp. 1051-1069

[View Record in Scopus](#)

[28]

M. Rutkowska, D. Macina, N. Mirocha-Kubień, Z. Piwowarska, L. Chmielarz

Appl. Catal. B Environ., 174 (2015), pp. 336-343

[ArticleDownload](#) [PDFView](#) [Record in Scopus](#)

[29]

M. Rutkowska, L. Chmielarz, M. Jabłońska, C.J. Van Oers, P. Cool

J. Porous Mater., 21 (2014), pp. 91-98

[CrossRefView](#) [Record in Scopus](#)

[30]

W.C. Yoo, X. Zhang, M. Tsapatsis, A. Stein

Microporous Mesoporous Mater., 149 (2012), pp. 147-157

ArticleDownload PDFView Record in Scopus

[31]

H. Mochizuki, T. Yokoi, H. Imai, S. Namba, J.N. Kondo, T. Tatsumi

Appl. Catal. A Gen., 449 (2012), pp. 188-197

ArticleDownload PDFView Record in Scopus

[32]

J. García-Martínez, K. Li

Mesoporous Zeolites, Preparation, Characterization and Applications (2012)

ISBN: 978-3-527-32638-8

[33]

J.-H. Kim, M.J. Park, S.J. Kim, O.-S. Joo, K.-D. Jung

Appl. Catal. A Gen., 264 (2004), pp. 37-41

ArticleDownload PDFCrossRefView Record in Scopus

[34]

K.A. Tarach, J. Martinez-Triguero, F. Rey, K. Góra-Marek

J. Catal., 339 (2016), pp. 256-296

View Record in Scopus

[35]

E.S. Shpiro, W. Grønert, R.W. Joyner, G.N. Baeva

Catal. Lett., 24 (1994), pp. 159-169

CrossRefView Record in Scopus

[36]

W. Grønert, N.W. Hayes, R.W. Joyner, E.S. Shpiro, M.R.H. Siddiqui, G.N. Baeva

J. Phys. Chem., 98 (1994), pp. 10832-10846

[37]

A. Corma, A. Palomares, F. Márquez

J. Catal., 170 (1997), pp. 132-139

ArticleDownload PDFView Record in Scopus

[38]

B. Wichterlová, J. Dédeček, A. Vondrová

J. Phys. Chem., 99 (1995), pp. 1065-1067

CrossRefView Record in Scopus

[39]

F. Bin, C. Song, G. Lv, J. Song, S. Wu, X. Li

Appl. Catal. B Environ., 150–151 (2014), pp. 532-543

ArticleDownload PDFView Record in Scopus

[40]

M.C. Nunes Amorim de Carvalho, F. Barboza Passos, M. Schmal

Appl. Catal. A Gen., 193 (2000), pp. 265-276

[41]

H. Praliaud, S. Mikhailenko, Z. Chajar, M. Primet

Appl. Catal. B Environ., 16 (1998), pp. 359-374

ArticleDownload PDFView Record in Scopus

[42]

A. Sultana, T. Nanba, M. Haneda, M. Sasaki, H. Hamada

Appl. Catal. B Environ., 101 (2010), pp. 61-67

ArticleDownload PDFView Record in Scopus

[43]

V. Petranovskii, E. Stoyanov, V. Gurin, N. Katada, M.-A. Hernandez, M. Avalos, A. Pestryakov,
F. Chávez Rivas, R. Zamorano Ulloa, R. Portillo

Rev. Mex. Fis., 52 (2013), pp. 170-185

View Record in Scopus

[44]

T. Zhang, J. Liu, D. Wang, Z. Zhao, Y. Wei, K. Cheng, G. Jiang, A. Duan

Appl. Catal. B Environ., 148–149 (2014), pp. 520-531

ArticleDownload PDFView Record in Scopus

[45]

L. Gang, J. van Grondelle, B.G. Anderson, R.A. van Santen

J. Catal., 186 (1999), pp. 100-109

[ArticleDownload](#) [PDFView](#) [Record in Scopus](#)

[46]

L. Li, F. Zhang, N. Guan, M. Richter, R. Fricke

Catal. Comm., 8 (2007), pp. 583-588

[ArticleDownload](#) [PDFView](#) [Record in Scopus](#)

[47]

A.L. Villa, C. Augusto Caro, C. Montes de Correa

J. Mol. Catal. A Chem., 228 (2005), pp. 233-240

[ArticleDownload](#) [PDFView](#) [Record in Scopus](#)

[48]

S. Yashnika, Z. Ismagilov

Appl. Catal. B Environ., 170–171 (2015), pp. 241-254

[49]

P.N.R. Vennestrøm, T.V.W. Janssens, A. Kustov, M. Grill, A. Puig-Molina, L.F. Lundegaard, R.R. Tiruvalam, P. Concepción, A. Corma

J. Catal., 309 (2014), pp. 477-490

[ArticleDownload](#) [PDFView](#) [Record in Scopus](#)

[50]

U. De La Torre, B. Pereda-Ayo, M. Romero-Sáez, A. Aranzabal, M.P. González-Marcos, J.A. González-Marcos, J.R. González-Velasco

Top. Catal., 56 (2013), pp. 215-221

[CrossRefView](#) [Record in Scopus](#)

[51]

T. Meng, N. Ren, Z. Ma

J. Mol. Catal. A Chem., 404–405 (2015), pp. 233-239

[ArticleDownload](#) [PDFView](#) [Record in Scopus](#)

[52]

T. Zhang, J. Shi, J. Liu, D. Wang, Z. Zhao, K. Cheng, J. Li

Appl. Surf. Sci., 375 (2016), pp. 186-195, 10.1016/j.apsusc.2016.03.049

[ArticleDownload](#) [PDFView](#) [Record in Scopus](#)

[53]

Z. Qin, L. Lakiss, J.-P. Gilson, K. Thomas, J.-M. Goupil, C. Fernandez, V. Valtchev

Chem. Mater., 25 (2013), pp. 2759-2766

CrossRefView Record in Scopus

[54]

L. Zhang, C. Zhang, H. He

J. Catal., 261 (2009), pp. 101-109

ArticleDownload PDFView Record in Scopus

[55]

G. Qi, J.E. Gatt, R.T. Yang

J. Catal., 226 (2004), pp. 120-128

ArticleDownload PDFView Record in Scopus

[56]

L. Chmielarz, A. Węgrzyn, M. Wojciechowska, S. Witkowski, M. Michalik

Catal. Lett., 141 (2011), pp. 1345-1354

CrossRefView Record in Scopus